

RESEARCH ARTICLE

New multi-standard dual-wideband and quad-wideband asymmetric step impedance resonator filters with wide stop band restriction

Yasir I. A. Al-Yasir  | Yuxiang Tu | Naser Ojaroudi Parchin | Ahmed M. Abdulkhaleq | Jamal Kosha | Atta Ullah | Raed A. Abd-Alhameed | James M. Noras

School of Electrical Engineering & Computer Science, University of Bradford, Bradford, UK

Correspondence

Raed A. Abd-Alhameed, School of Electrical Engineering & Computer Science, University of Bradford, Bradford, UK.
Email: r.a.a.abd@bradford.ac.uk

Funding information

Horizon 2020 Framework Programme (European Union), Grant/Award Number: H2020-MSCA-ITN-2016 SECRET-722 424

Abstract

New multi-standard wide band filters with compact sizes are designed for wireless communication devices. The proposed structures realize dual-wideband and quad-wideband characteristics by using a new skew-symmetrical coupled pair of asymmetric stepped impedance resonators, combined with other structures. The first and second dual-wideband filters realize fractional bandwidths (FBW) of 43.2%/31.9% at the central frequencies (CF) of 1.875/1.63 GHz, and second bandwidths of 580 MHz/1.75 GHz at CF of 5.52/4.46 GHz, respectively. The proposed quad-band filter realizes its first/second/third/fourth pass bands at CF 2.13/5.25/7.685/9.31 GHz with FBW of 46.0%/11.4%/4.6% and 5.4%, respectively. The wide pass bands are attributed to the mutual coupling of the modified ASIR resonators and their bandwidths are controllable by tuning relative parameters while the wide stop band performance is optimized by the novel interdigital cross coupled line structure and parallel uncoupled microstrip line structure. Moreover, the quad band is generated by introducing the novel defected rectangle structure. These multi-standard filters are simulated, fabricated and measured, and measured results agree well with both simulated results and theory predictions. The good in-band and out-of-band performances, the miniaturized sizes and simple structures of the proposed filters make them very promising for applications in future multi-standard wireless communication.

KEYWORDS

asymmetrical stepped-impedance resonator (ASIR), dual-wide band, multi-standard, quad-wide band bandpass filter (BPF), wide stopband

1 | INTRODUCTION

Ever-increasing demand for compact wireless transceivers continues to impact the field of microwave and radio frequency communication.^{1,2} One of the most important modules in such systems is the filter,³⁻²² and its performance dominates the whole wireless communication system.

Compared to the traditional stepped impedance resonator (SIR) with two step discontinuities, the asymmetric SIR has only one discontinuity but retains the characteristic of controllable spurious modes.

It has advantages of compact size, less loss, and versatility in design, particularly for high-order BPFs such as dual band, triple band and quad band BPFs because of its

inherently higher order resonant modes. It has recently been used to construct high-performance BPFs,³⁻⁷ and in References 6,7, two-stage wide-stopband BPFs using asymmetric SIRs have been proposed. The schemes of distributing spurious resonant frequencies of asymmetric SIR with wide stop band performance are realized. Additionally, with fewer discontinuities, the asymmetric SIR can be easily folded and coupled, and this results in a lower insertion loss and greater size reduction.

On the other hand, with the current increasingly stringent limitations on frequency spectrum resources and the development of advanced multi-standard wireless communication systems, multi-standard internal filters have become a necessity for state-of-the-art multifunction “smart phones” and wireless transceivers for mobile devices. Such filters are generally required to be capable of covering the frequency bands of the Global Positioning System (GPS: band centered at 1.57 GHz), the Global System for Mobile Communication (GSM: 1800/1900 MHz etc.) and the Universal Mobile Telecommunications System (UMTS: 1710-1880/1850-1990/1920-2170 MHz etc.). Moreover the ever expanding implementation of the Wireless Local Area Network (WLAN) adds the requirement of a band centered at 2.4 GHz and/or 5.2 GHz. Many dual band filters have recently been designed to satisfy such demanding requirements. However, many of these that are also miniaturized fail to fully cover all the required bands, especially at the lower frequencies due to the narrower dual bandwidth,^{3-5,9,16} or their size or thickness makes them difficult to integrate within mobile devices or portable wireless modules.^{7,12,13,15}

In this article, we propose novel multi-standard asymmetric SIR filters including both dual-wideband filters with wide stopbands and a quad-wideband filter. These filters are capable of generating two and four wide operating bands that effectively cover the GPS/GSM/UMTS/IEEE802.11a application in mobile devices, including GPS (1.75 GHz), GSM1800 (1710-1880 MHz), GSM1900 (1850-1990 MHz), UMTS (1920-2170 MHz), and IEEE 802.11a (5 GHz) bands. Meanwhile, in-band and out-of-band performance of the proposed filters is further enhanced by novel structures. To the best of authors' knowledge, these structures realize for the first time dual wideband and wide stop band resulting from the restriction of high order harmonic frequencies at the same time in dual wideband^{8,10,11,13-15} and asymmetric SIR filters.³⁻⁷ Moreover, the proposed structures use the capacitive coupling of only two miniaturized resonators to realize dual-wideband and quad-wideband responses without such extra structures such as via holes or defected ground planes, and so are unique among dual-wideband and quad-wideband filters.^{10-13,15} The filters are simulated and optimized using CST microwave studio software.²³

2 | RESONANCE CHARACTERISTICS OF THE ASYMMETRIC SIR UNIT AND THE SKEW-SYMMETRICAL ASYMMETRIC SIR COUPLED PAIR

2.1 | Characteristic of the asymmetric SIR unit

The asymmetric SIR shown in Figure 1, adopted from Reference 4, consists of sections with low and high characteristic impedances Z_1 and Z_2 . The physical lengths L_1 and L_2 , physical widths W_1 and W_2 , and electrical lengths θ_1 and θ_2 are shown for the two sections with Z_1 and Z_2 , respectively. The characteristic impedance ratio K and the length ratio α are defined as follows:

$$K = \frac{Z_2}{Z_1} \quad (1)$$

$$\alpha = \frac{\theta_2}{\theta_1 + \theta_2} \quad (2)$$

where α is located in the range of (0, 1).

The input admittance Y_{in} of the proposed asymmetric SIR unit is derived as:

$$Y_{in} = \frac{j K \tan \theta_1 + \tan \theta_2}{Z_2 (1 - K \tan \theta_1 \tan \theta_2)} \quad (3)$$

It is known that resonance of the proposed asymmetric SIR occurs when $Y_{in} = 0$. Based on Equation (3), this resonance happens when

$$\frac{K \tan \theta_1 + \tan \theta_2}{1 - K \tan \theta_1 \tan \theta_2} = 0 \quad (4)$$

From the solution of Equation (4), the first and second spurious frequencies f_{s1} and f_{s2} are plotted in Figure 2, normalized by the fundamental frequency against α with different values of K . When α is more than 0.5, the normalized

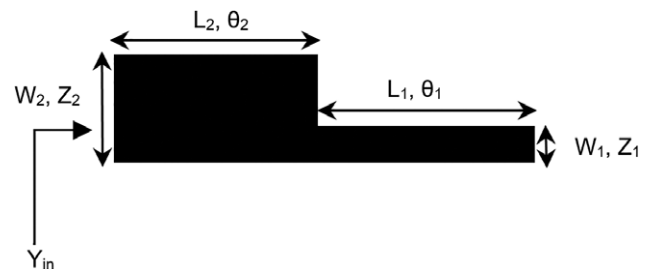
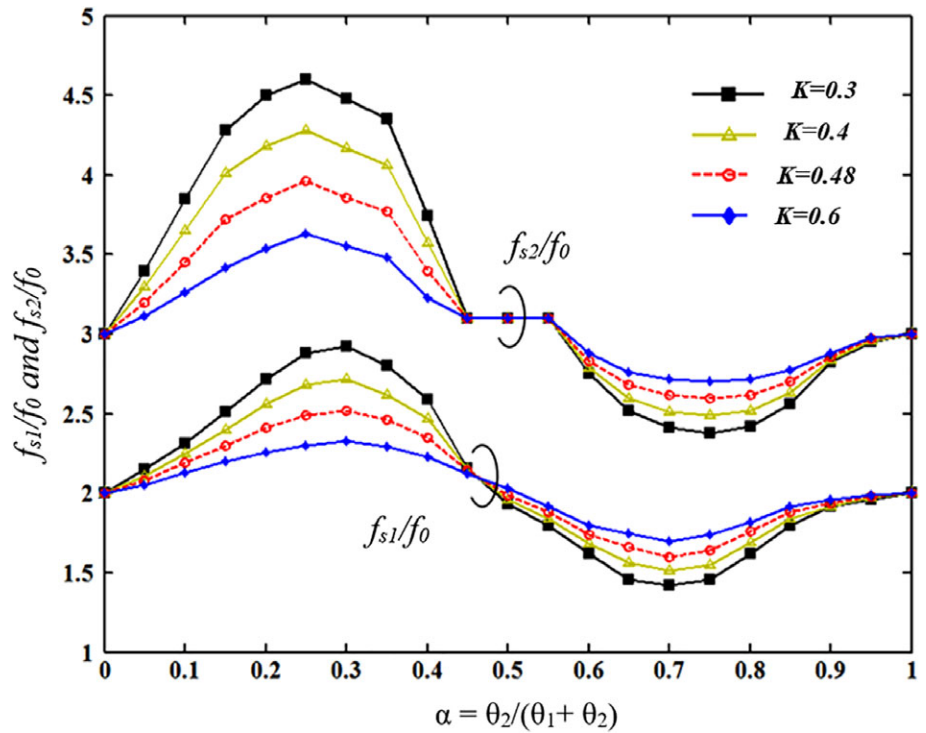


FIGURE 1 Structure of an asymmetric SIR⁴

FIGURE 2 f_{s1} (the first spurious frequency) and f_{s2} (the second spurious frequency) normalized by f_0 (the fundamental frequency) for the asymmetric SIR in Figure 1



frequency f_{s1}/f_0 is greater than 2 and f_{s2}/f_0 is greater than 3, respectively. Also smaller K can result in greater normalized frequency when α is fixed. When α is greater than 0.5, the normalized frequency f_{s1}/f_0 is less than 2 and f_{s2}/f_0 is less than 3. Smaller K can result in lower normalized frequency for a fixed α . When $K = 1$, f_{s1}/f_0 is equal to 2 and f_{s2}/f_0 is equal to 3. This means that in this limit a uniform impedance resonator is realized and the high order resonant frequency is an integer multiple of the fundamental frequency f_0 . Therefore, the higher order spurious resonant modes, which depend on the choice of the characteristic impedance ratio K and the electric length ratio α , can be found by combining Equations (2) and (4).

2.2 | Characteristic of the skew-symmetrical asymmetric SIR coupled pair

A skew-symmetrical asymmetric SIR coupled pair is illustrated in Figure 3. It contains two asymmetric SIR units connected through two high impedance coupled lines.

The coupling matrix referred to in Reference 16 will not be discussed in this article because of its non-wideband

limitation.^{16,17} The coupling between two ASIRs can be represented by a J-inverter susceptance $\overline{J}_{1,2}$ where the subscript 1 and 2 denotes the first and second passband. A larger value of $\overline{J}_{1,2}$ means a stronger coupling strength between two ASIRs. The normalized $\overline{J}_{1,2}$ can be determined by

$$\overline{J}_{1,2} = J_{1,2} Z_0 \quad (5)$$

where Z_0 represents the referred port impedance.

The external quality factor $Q_{ex1,2}$ and the normalized J-inverter susceptance $\overline{J}_{1,2}$ can be related by Reference 16.

$$Q_{ex1,2} = \frac{\pi}{2\overline{J}_{1,2}^2} \quad (6)$$

The external quality factor $Q_{ex1,2}$ can be further extracted by

$$Q_{ex1,2} = \frac{f_{c1,2}}{\Delta_{1,2}} = \frac{f_{c1,2}}{\Delta_{(\pm\frac{\pi}{2})1,2}} \quad (7)$$

where $f_{c1,2}$, $\Delta_{1,2}$, $\Delta_{(\pm\frac{\pi}{2})1,2}$, represents the central frequency, -3 dB bandwidths, and the frequency bandwidth of phase curve changing $(\pm\frac{\pi}{2})$ with respect to $f_{c1,2}$, respectively. $\overline{J}_{1,2}$ can be calculated by substituting the extracted $Q_{ex1,2}$ into Equations (6) and (7).

From the full-wave EM simulation (CST software²³), it is noted that the frequency response performance (in terms of

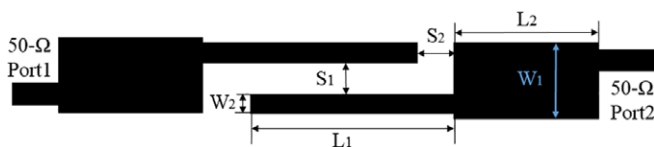


FIGURE 3 Structure of a skew-symmetrical asymmetric SIR coupled pair

TABLE 1 The transformation relationship of in-band performance of skew-symmetrical asymmetric SIR coupled pair and asymmetric SIR unit. “Improved” means significant enhancement of performance at relative frequency; “NC/DE” means no significant change or degradation of performance at relative frequency point. When α ranges from 0.3 to 0.7

α	f The fundamental frequency f_0	The first spurious frequency f_{s1}	The second spurious frequency f_{s2}	The third spurious frequency f_{s3}	The fourth spurious frequency f_{s4}
0.3	NC/DE	Improved	NC/DE	Improved	NC/DE
0.4	Improved	NC/DE	Improved	NC/DE	Improved
0.42	Improved	NC/DE	Improved	NC/DE	Improved
0.5	Improved	NC/DE	Improved	NC/DE	Improved
0.55	Improved	NC/DE	NC/DE	Improved	NC/DE
0.6	Improved	Improved	NC/DE	Improved	NC/DE
0.65	Improved	Improved	NC/DE	NC/DE	Improved
0.7	Improved	Improved	NC/DE	NC/DE	NC/DE

bandwidth, return loss and insertion loss) is improved significantly at some frequency points in the SS-ASIR coupled pair while in other respects the performance is not changed much or degraded in comparison with the asymmetric SIR unit. Table 1 shows the frequency response transformation from asymmetric SIR unit to skew-symmetrical asymmetric SIR coupled pair. It can be seen that when the asymmetric SIR's electric length ratio α ranges from 0.4 to 0.5, the frequency response at frequency f_0 , f_{s3} and f_{s4} enhances significantly in the SS-ASIR coupled structure, while it does not change much or degrades at f_{s1} and f_{s3} . When $\alpha = 0.6$, the frequency response at f_0 , f_{s1} , and f_{s3} enhances greatly, but it does not vary much or degrades at f_{s2} and f_{s4} . The transformation table is useful to analysis and transform frequency bands where the performance-enhanced frequency response appears into desired pass bands by considering the asymmetric SIR unit characteristic. It is also useful to analyze and transform frequency bands where the performance-degraded frequency response appears into stop bands or excite them to become pass band by modifying the SS-ASIR coupled structure.

2.3 | The influence of electric length ratio α in SS-ASIRs

An inherent property of the skew-symmetrical asymmetric SIR (SS-ASIR) coupled pair is that the resonant frequency location and bandwidth performance are mainly influenced by the electric length ratio α when length L_1 is fixed, and is hardly affected by the impedance ratio K . This invariance characteristic is not found with the asymmetric SIR unit, where the normalized frequency (and resonant frequency) is closely related with K value. This characteristic of $\alpha = 0.42$ is shown in Figure 4: resonant frequency locations and their bandwidths are nearly fixed when α is fixed at 0.42, and

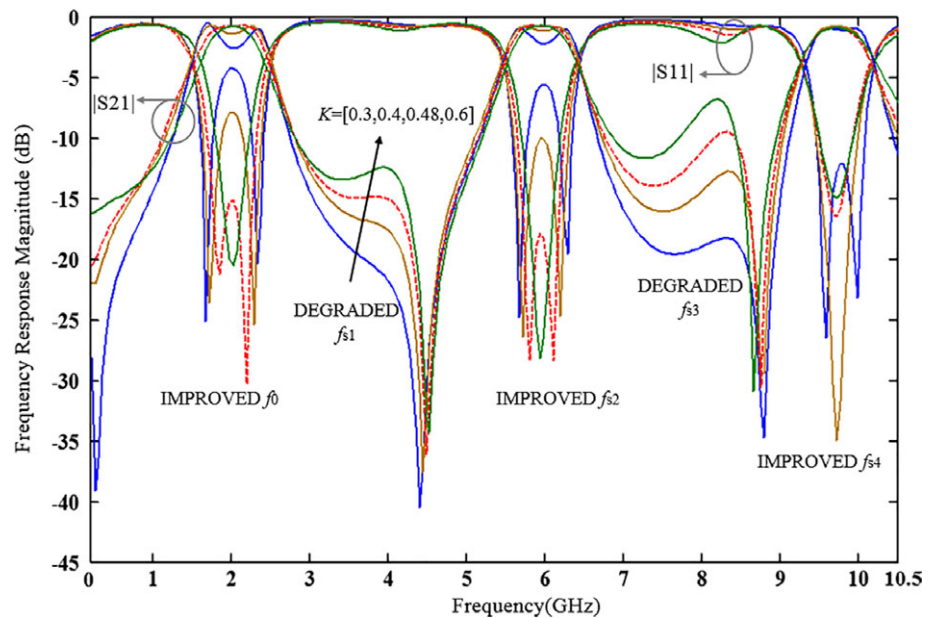
these two parameters are little influenced by K . Similar phenomenon can be observed when α is fixed at other values. This means α is the main factor to influence the horizontal frequency response performance such as resonant frequency locations and bandwidths in SS-ASIR coupled structures.

2.4 | The influence of impedance ratio K in SS-ASIRs

The return loss and insertion loss performance of enhanced f_0 and f_{s2} (seen in Table 1 and Figure 4) becomes better when K varies from 0.3 to 0.6. Meanwhile, the return loss and insertion loss performance of degraded f_{s1} and f_{s3} (seen in Table 1 and Figure 4) become better and forms two spurious peaking finally. Similar phenomenon can be observed when K takes other values. Therefore, the impedance ratio K is a major influence on the vertical frequency response performance such as return loss and insertion loss in both pass-band and stop-band of SS-ASIR coupled structures. By considering the characteristic of SS-ASIR coupled pairs and of the asymmetric SIR unit, $\alpha = 0.42$ and $K = 0.48$ are extracted to design the proposed filters. The performance-enhanced frequency bands at f_0 and f_{s2} are used to form the first and second pass band in the proposed dual-band and quad-band filters. The performance-degraded frequency band at f_{s3} and performance-enhanced frequency band at f_{s4} are unwanted in the proposed dual-band filters, but they are used to form the third and fourth pass band in the proposed quad-band filter.

Figure 5 plots the variation of coupling bandwidth as a function of the gap size (S_1) between the two resonators. Increasing the gap between the resonators reduces the coupling bandwidth of the designed filter and vice versa. Given the required electrical length ratio α , coupling coefficients and external quality factor for the proposed filters, one may determine the proper specifications based on these factors.

FIGURE 4 Frequency characteristic curves of the SS-ASIR coupled pair when $\alpha = 0.42$, $L_1 = 11$ mm and $K = 0.3, 0.4, 0.48$, and 0.6



3 | THE MODIFIED SKEW-SYMMETRICAL ASYMMETRIC SIR FILTER

3.1 | SS-ASIR filter with open stub and folded coupled lines

In the skew-symmetrical asymmetric SIR filter, open stubs can be added to the low impedance lines, and the high impedance coupled lines can be folded, to achieve optimized performance. This geometry and its equivalent circuit are shown in Figures 6 and 7, respectively. When two open stubs are moved from point A to C, the suppression performance of f_{s3} and f_{s4} becomes progressively better while the return loss performance of f_{s2} become worse from A to B and better from B to C. Meanwhile, the insertion loss and return loss performance of fundamental frequency f_0 remains almost the same. Therefore, two open stubs are placed at

point C. Figure 8 shows the open stub effect on the frequency response of the SS-ASIR filter.

The high impedance lines are also folded to form the section of length H_1 between the high and low impedance lines. Compared to conventional coupled lines that are not folded, the suppression of unwanted transmission at frequency f_{s4} is greatly improved when the interval H_1 varies from 0.5 mm to 0.9 mm. The change in the frequency response for this variation of H_1 is plotted in Figure 9.

The design procedures for dual- and quint-wideband type BPFs can be summarized as follows:

1. Choose a suitable electrical length ratio α , thus setting the fundamental frequency f_0 , and choose the characteristic impedance ratio K in the ASIR to improve insertion loss and return loss performance.
2. Analyze the transmission zero generating requirement of the interdigital cross-coupled line section added to the SS-ASIR structure and find suitable transmission zero locations.
3. According to previous results, tune the length of the interdigital cross-coupled line section to meet the required S_{21} to form a wide stop band for the dual-wideband type ASIR filter. The gap parameter S_5 is also tuned for optimized results.

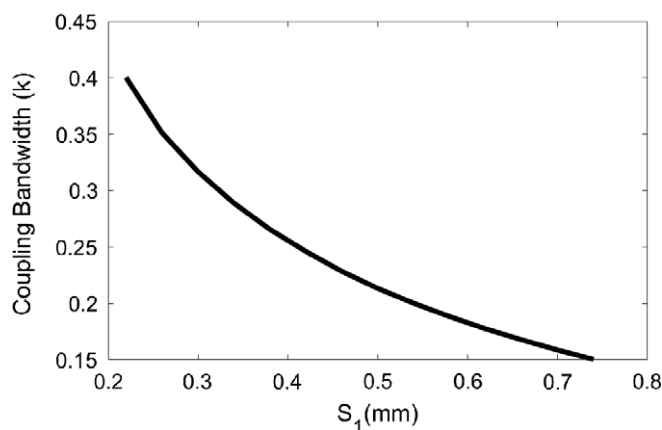


FIGURE 5 Coupling bandwidth (K) with the gap size (S_1)

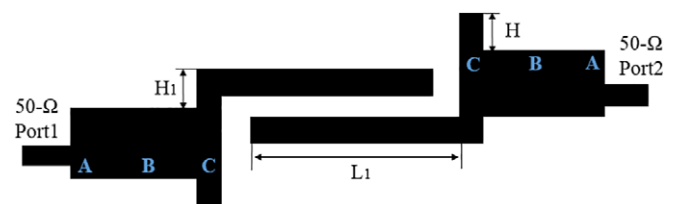


FIGURE 6 Schematic diagram of an SS-ASIR filter with open stubs and folded coupled lines

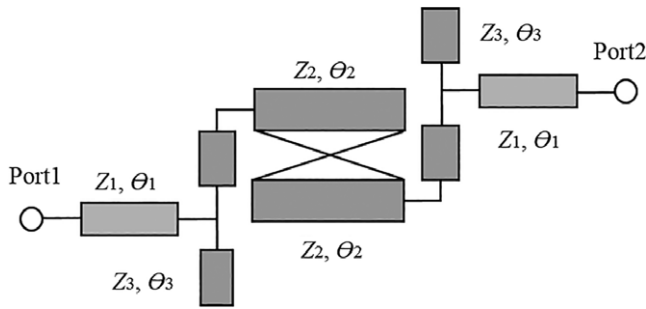


FIGURE 7 The equivalent circuit of an SS-ASIR filter with open stubs and folded coupled lines

4. Tune the length of the interdigital cross-coupled line section to enable a multi-band response with good isolation between operating bands.

5. The same design steps can be applied for the quint-wideband type BPF.

Because of the non-wideband limitation of the coupling matrix, coupling coefficients are not important in this design, while the external quality factor Q_{ex} can be discussed for performance optimization, as mentioned above.

3.2 | The modified SS-ASIR filter with interdigital cross-coupled line (ICCL)

To further optimize the in-band and out-of-band performance of the proposed dual-band filter, auxiliary interdigital cross-coupled lines whose width and length are W_5 and L_5 are utilized to realize multi-path coupling between two

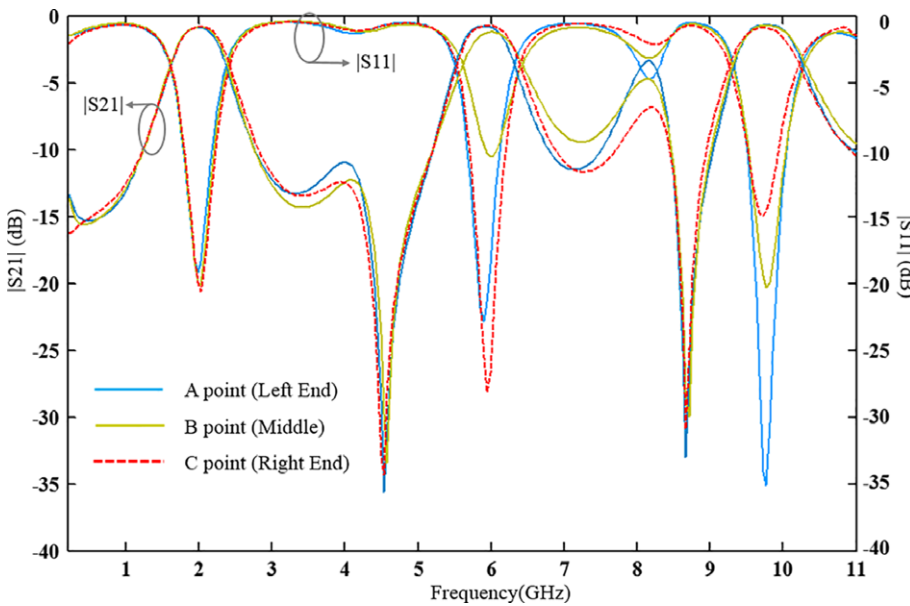


FIGURE 8 The open stub effect on the frequency response of the SS-ASIR filter

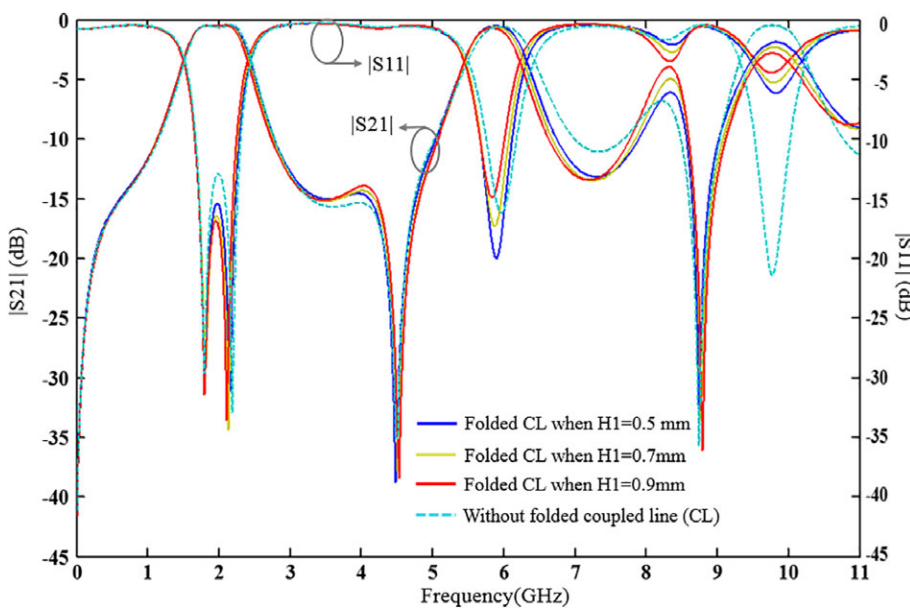


FIGURE 9 The frequency response of the modified SS-ASIR filter vs frequency when H_1 varies from 0.5 mm to 0.9 mm

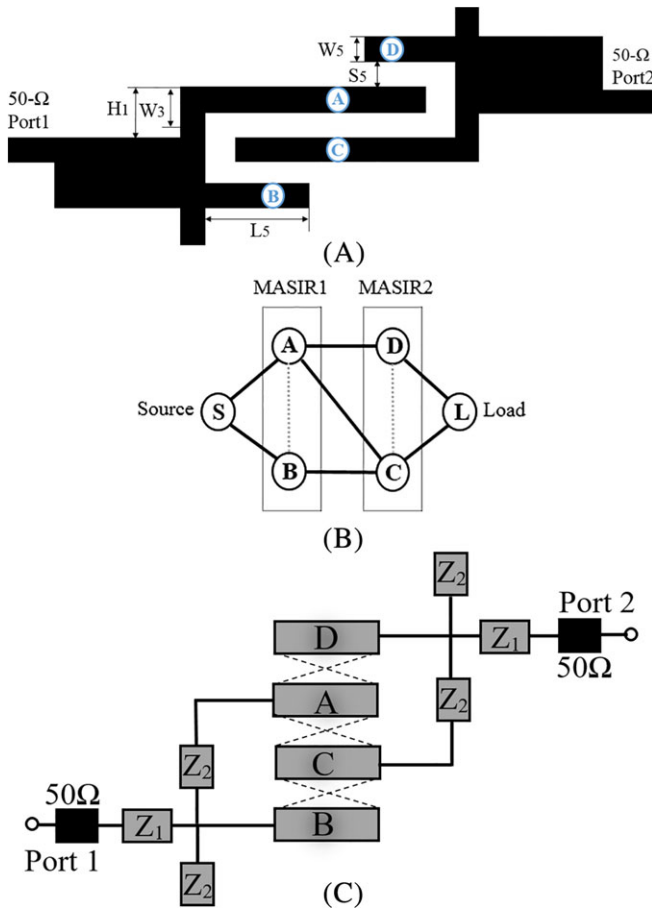


FIGURE 10 Schematic diagram of the modified SS-ASIR coupled pair with interdigital cross coupled lines. (A) Structure. (B) Coupling routing scheme. A, B denotes the main coupling line and auxiliary cross coupling in MASIR1, respectively. C, D denotes the main coupling line and auxiliary cross coupling in MASIR2, respectively. (C) Equivalent circuit and coupling routing scheme for the SS-ASIRs with ICCLs

modified ASIRs (MASIRs), as seen in Figure 10. Compared to the single coupling route of A-C, at least two extra coupling routes including A-D and B-C are created by the inclusion of the auxiliary coupled lines. This interdigital multipath coupling scheme of the modified SS-ASIR filter is shown in Figure 10B. Moreover, because of the small distance between the main and auxiliary coupled lines, mutual coupling of A-B and C-D exists at the same time. This coupling is illustrated as dashed gray lines in Figure 10B.

By including auxiliary coupled lines, the filter's out-of-band spurious frequency suppression performance and pass-band selectivity is considerably improved. The designed dual-band band pass filter (BPF) adopting an interdigital cross-coupled configuration produces a transmission zero (TZ) to approach f_{s3} and f_{s4} . The transmission zero occurs because of cancellation of the transmitted signals passing through different routes. The transmission line equivalent circuit model and the coupling routing scheme for the SS-ASIRs are shown in Figure 10C. The impedance values of the transmission lines are: $Z_1 = 73.4856 \Omega$, $Z_2 = 23.5845 \Omega$, $Z_A = Z_C = 67.0065 \Omega$, and $Z_B = Z_D = 73.5209 \Omega$, these values have been achieved and verified with the aid of the spice extraction tool embedded in the CST software.^{17,23}

As seen in Figure 11, when the length of auxiliary coupled line L_5 ranges from 1.4 to 1.8 mm, optimized suppression of f_{s3} and f_{s4} is achieved. Also a wide stop band ranging from 6.3 to 12 GHz at the upper side of the second pass band is realized simultaneously. Also, the second pass band upper side's selectivity is improved with the two pass bands' return loss and insertion loss performance unaffected. Figure 12 plots Q_{ex1} , Q_{ex2} , f_{s2}/f_0 and Q_{ex2}/Q_{ex1} vs S_5 , which is the gap between auxiliary coupled line and main coupled line in the interdigital cross-coupled SS-ASIR filter. When

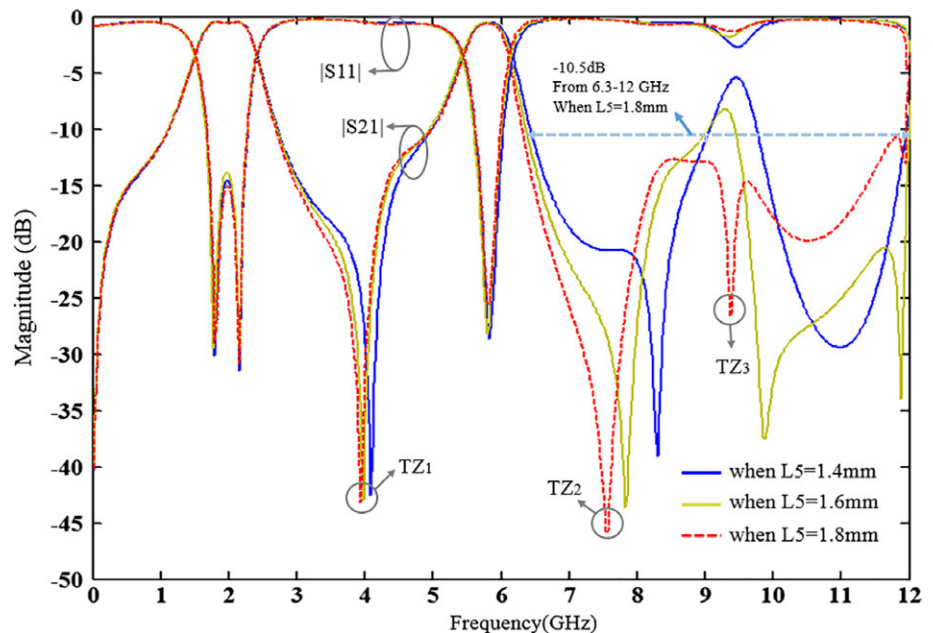


FIGURE 11 The effect of L_5 on the interdigital cross-coupled SS-ASIR

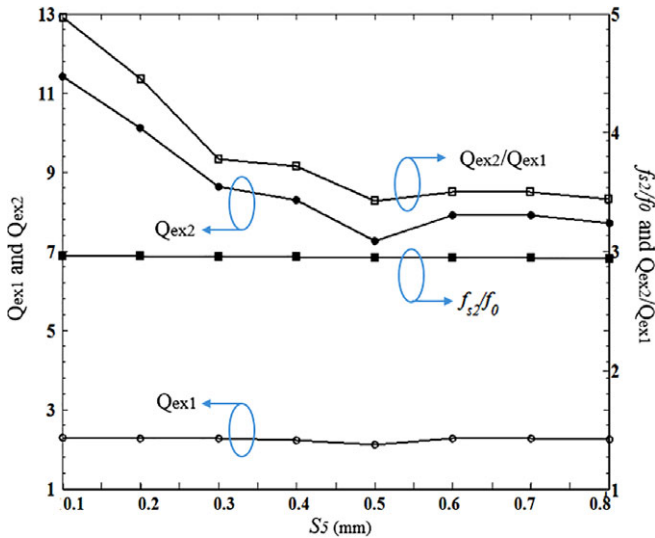


FIGURE 12 Q_{ex1} , Q_{ex2} , f_{s2}/f_0 and Q_{ex2}/Q_{ex1} vs S_5

S_5 changes from 0.1 mm to 0.8 mm, Q_{ex1} and f_{s2}/f_0 remain almost the same. This exhibits the stable invariance property of resonant frequency location in the SS-ASIR coupled structure and coincides with the frequency response in Figure 4. Q_{ex2} decreases initially and increases a little later: this means that the bandwidth of f_{s2} can be controlled and expanded by tuning S_5 . Therefore, S_5 is a factor that can tune Q_{ex2} and $\overline{J}_{1,2}$ in SS-ASIRs with the interdigital cross coupled line structure.

The proposed filters were fabricated on an RO3010 substrate with a relative permittivity of 10.2, and measured using an HP8550 vector network analyzer. The simulated S -parameters, measured S -parameters and photograph of the hardware realization of the designed dual-wideband SS-ASIRs with ICCLs are plotted in Figure 13. Good agreement is observed between the

TABLE 2 Parameters of the proposed four types of modified SS-ASIR filters. All dimensions are in millimeters

Filter type parameter	The modified SS-ASIR filter	The modified SS-ASIR filter with ICCLs	The modified SS-ASIR filter with PUMLS	The modified SS-ASIR filter with DRS
L_1	11	11	11	11
L_2	15.6	15.6	15.6	15.6
W_1	1.6	1.6	1.6	1.6
W_3	0.4	0.4	0.4	0.4
L_5		1.81		
S_5		0.25		
W_5		0.42		
L_r			7.05	
L_m			2.32	
W_m			0.07	
R_d				0.6
W_d				4.65
H_d				1.2

simulated and measured results and the slight discrepancies are attributed to losses and fabrication errors. Dual wide bands are realized with good in-band return loss performance. The first pass band ranges from 1.47 to 2.28 GHz with central frequency of 1.875 GHz, bandwidth of 810 MHz and fractional band width (FBW) of 43.2%. It can be applied in the application of Global Positioning System (GPS: frequency band centered at 1.57 GHz), Global System for Mobile Communication (GSM: 1800/1900 MHz) and Universal Mobile Telecommunication System (UMTS: 1710-1880/1850-1990/1920-2170 MHz etc.).

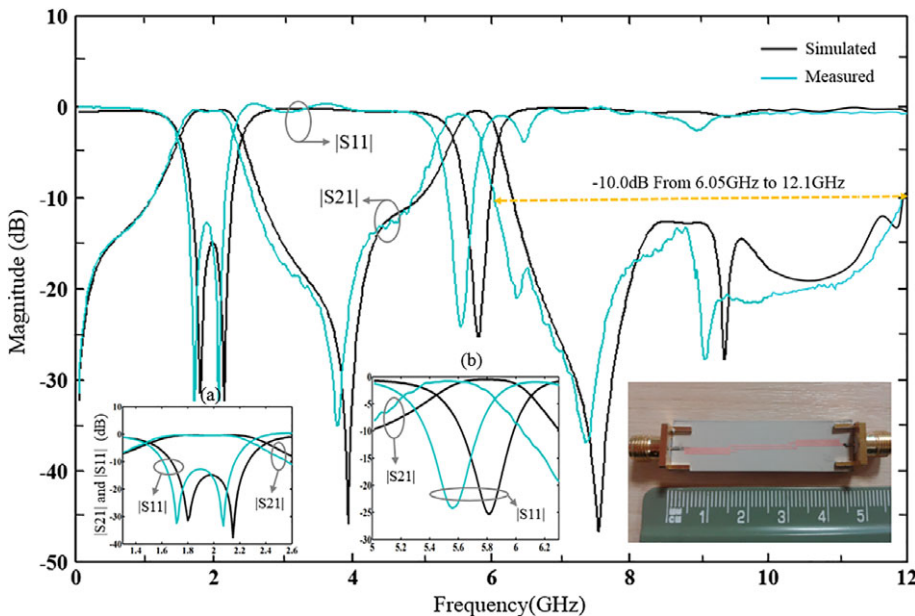


FIGURE 13 Simulated, measured results and photograph of the hardware realization of an SS-ASIR with ICCLs. (A) Narrowband view of the first passband. (B) Narrowband view of the second passband

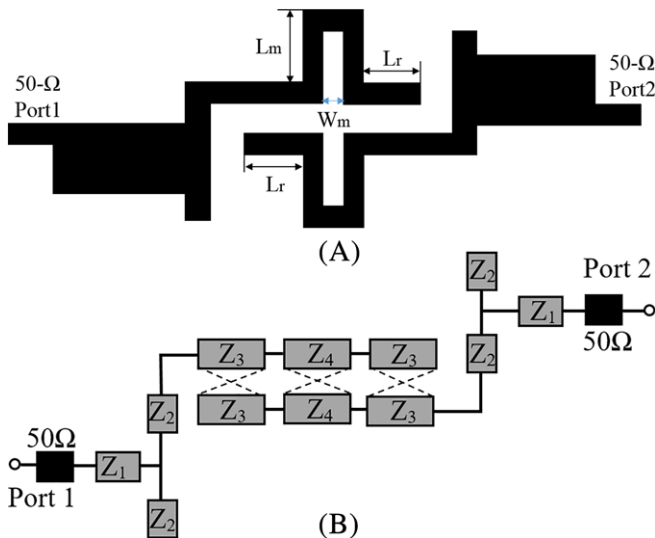


FIGURE 14 (A) Schematic diagram of the proposed modified SS-ASIR filter with parallel uncoupled microstrip lines. (B) Equivalent circuit and coupling routing scheme for the SS-ASIR filter with PUMLS

The second pass band ranges from 5.23 to 5.81 GHz with central frequency of 5.52 GHz, bandwidth of 580 MHz and fractional band width (FBW) of 10.5%. It can be applied in IEEE802.11a WLAN applications including 5G Wi-Fi. Moreover, good insulation is achieved between two pass bands, eliminating signal interference between dual-bands. The stop band ranges from 2.56 to 4.86 GHz with -10 dB suppression. Due to the adoption of the interdigital cross-coupled line structure, an extra transmission zero near f_{s3} and f_{s4} is created. A wide upper stop band ranging from 6.05 to 12.1 GHz with -10 dB suppression is generated, which can be seen in Figure 13.

Parameters of the modified SS-ASIR filter and modified SS-ASIR filter with interdigital cross coupled lines (ICCLs) are shown in Table 2.

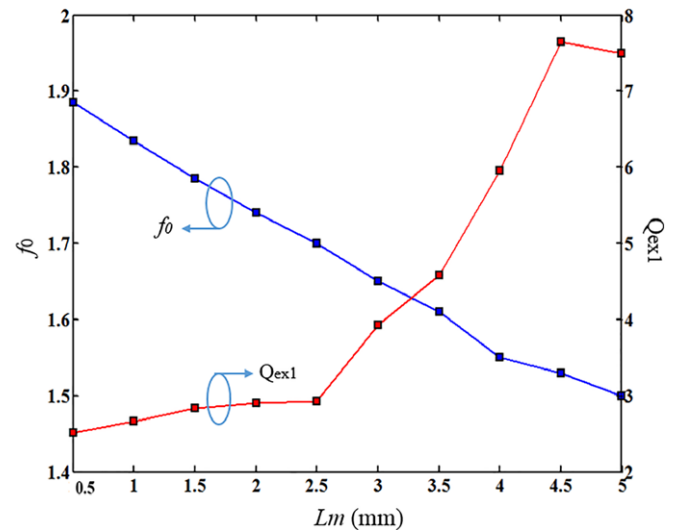


FIGURE 16 f_0 and Q_{ex1} vs against L_m

3.3 | The modified SS-ASIR filter with parallel uncoupled microstrip lines (PUMLS)

An uncoupled section located within conventional coupled lines is a useful method to achieve extra transmission zeros close to existing zeros created by the conventional coupled lines. Therefore, the results extending the stopband bandwidth with a better suppression level can be achieved. At the same time, this method can also give freedom to optimize the in-band performance of the original structure. Figure 14 shows the topological structure of the proposed modified SS-ASIR filter with parallel uncoupled microstrip lines. These parallel uncoupled microstrip lines are formed by bending the original coupled lines outwards. The parallel uncoupled microstrip line's reference location to the original coupled line open end is L_r . The parallel uncoupled microstrip line height and inner gap is L_m and W_m , respectively. The same procedure applied to achieve the equivalent circuit

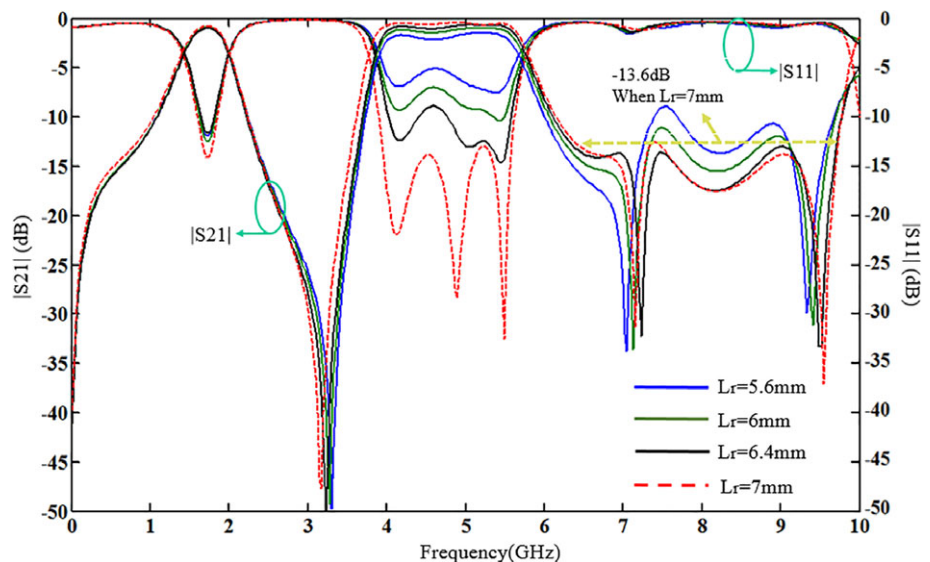


FIGURE 15 L_r 's impact on the frequency response of the SS-ASIR filter with PUMLS

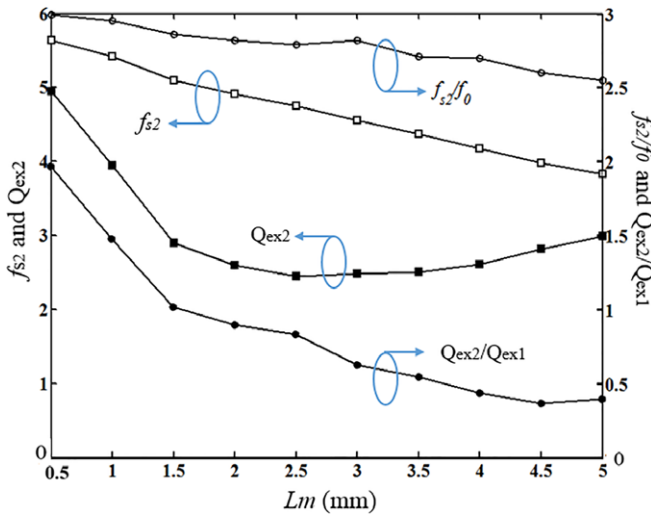


FIGURE 17 f_{s2} , Q_{ex2} , f_{s2}/f_0 and Q_{ex2}/Q_{ex1} vs against L_m

elements used in Figure 10C, is adopted for the SS-ASIR filter with PUMs as shown in Figure 14B. The impedance values of the transmission lines are: $Z_1 = 73.4856 \Omega$, $Z_2 = 23.5845 \Omega$, $Z_3 = 67.4162 \Omega$, and $Z_4 = 58.6799 \Omega$.

Compared to the former modified SS-ASIR filter with its interdigital cross-coupled line structure, the wider second pass band is achieved by adopting novel parallel uncoupled microstrip lines. In the former structure, Q_{ex1} and Q_{ex2} are equal to 2.28 and 9.37 when $S_5 = 0.25$ mm (as shown in Figure 11), while $Q_{ex1,2}$ equal 2.71 and 3.48 when $L_m = 2.3$ mm in this novel filter with PUMs. This means \bar{J}_2 is improved greatly and a stronger coupling strength between two modified ASIRs is realized. Figure 15 shows

the impact of the reference location parameter L_r on the frequency response of the filter with parallel uncoupled microstrip lines. It is noted that when L_r changes from 5.6 mm to 7 mm, the second pass band return loss performance is enhanced considerably and its bandwidth becomes wider resulting in forming a wide second pass band of more than 1.5 GHz. Meanwhile, the frequency response of the first pass band does not vary much. Hence, L_r is a vital factor to influence \bar{J}_2 and Q_{ex2} . Moreover, the parallel uncoupled microstrip line structure achieves one extra transmission zero nearby f_{s3} and f_{s4} , leading to an extended wide stopband bandwidth with better suppression level, as seen in Figure 15.

Figures 16 and 17 show the impact of L_m on the frequency response of the SS-ASIR filter with PUMs. In Figure 16, when L_m ranges from 0.5 mm to 5 mm, the fundamental frequency f_0 decreases continuously while Q_{ex1} increases slightly at first and increases dramatically when L_m is greater than 2.5 mm. This shows that the parallel uncoupled microstrip line height L_m can increase Q_{ex1} and decrease \bar{J}_2 within a certain range. Figure 17 plots the f_{s2} , Q_{ex2} , f_{s2}/f_0 and Q_{ex2}/Q_{ex1} vs against L_m . When L_m ranges from 0.5 mm to 1.5 mm, the rate of decline of Q_{ex2} is much faster than the rate of decline of f_{s2} , which means the bandwidth centered at f_{s2} is growing rapidly. When L_m ranges from 1.5 mm to 2.5 mm, the rate of decline of Q_{ex2} is almost the same as that of f_{s2} , that means that a wide band width centered at f_{s2} is formed and does not change much. When L_m ranges from 2.5 mm to 5 mm, Q_{ex2} increases as f_{s2} decreases, which means that the band centered at f_{s2} becomes narrower. In the whole process, f_{s2} moves from

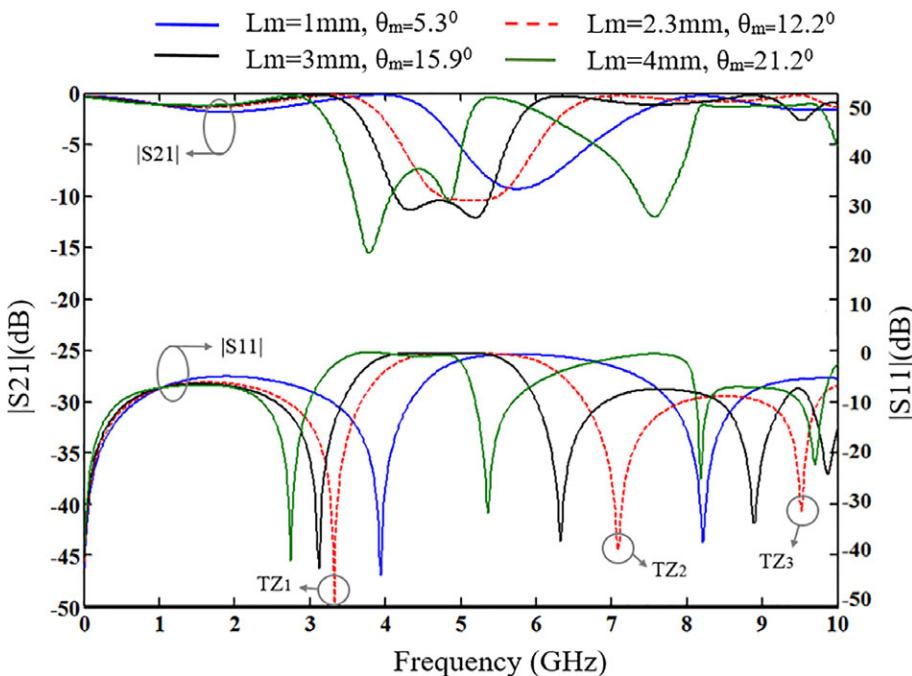
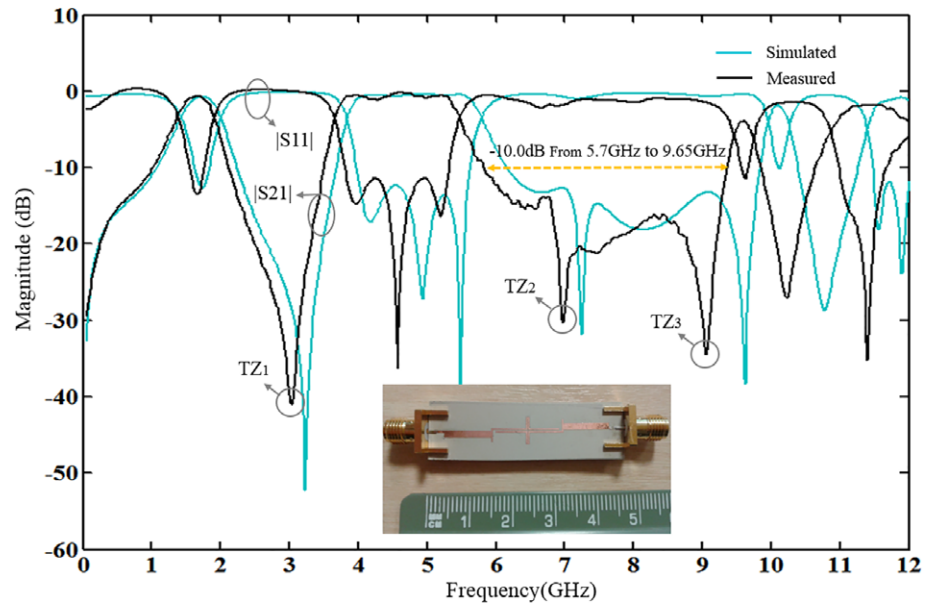


FIGURE 18 The analysis of the PUM unit

FIGURE 19 Simulated, measured results and photograph of the hardware realization of an SS-ASIR with PUMLS



5.6 GHz to 3.8 GHz with the second pass band being expanded to more than 1.5 GHz. Hence, L_m is also a factor to influence Q_{ex2} and strengthen \overline{J}_2 .

The reason for this can be explained by analyzing the parallel uncoupled microstrip line unit, whose topological structure and frequency response are plotted in Figure 18. As seen in the figure, the PUML unit forms a wide pass band of more than 1 GHz when L_m changes from 1 mm to 3 mm, and the pass band central frequency can be tuned by L_m . This result proves the advantage of the PUML structure to optimize the in-band performance of the filter. As for out-of-band performance, the PUML unit generates three transmission zeros (TZs) at both sides of the pass band, as plotted in Figure 18. These three TZs can improve the isolation

performance between two pass bands and the suppression level of undesired f_{s3} and f_{s4} .

The simulated S -parameters, measured S -parameters and photograph of the hardware realization of the designed dual-wideband SS-ASIRs with PUMLS are plotted in Figure 19. There is good agreement between the simulated and measured results and the slight discrepancies are attributed to losses and fabrication errors. It can be seen that dual wide bands are realized with good in-band return loss performance. The first pass band ranges from 1.37 to 1.89 GHz with central frequency of 1.63 GHz, bandwidth of 520 MHz and fractional band width (FBW) of 31.9%. It can be applied in the application of Global Positioning System (GPS: frequency band centered at 1.57 GHz), Global System for

TABLE 3 Performance comparison to the proposed of modified SS-ASIR filter with (A) ICCLS and (B) PUMLS. All dimensions are in millimeters

Reference	CF (GHz)	−3 dB FBW (%)	RL at CF (dB)	IL at CF (dB)	Size	No. of transmission poles in each passband	Wide stop band restriction
8	2.4/5.26	13.7/6.3	28/12	0.6/1.4	$0.46\lambda_g \times 0.42\lambda_g$	2/2	no
9	2.43/3.73	4.5/6.1	24/24	2.5/1.3	$0.43\lambda_g \times 0.69\lambda_g$	1/1	No
15	2.4/3.5	6.88/8.57	26/16	<0.3	$0.25\lambda_g \times 0.4\lambda_g$	2/2	No
18	5/8	50/12.5	24/35	1/1.2	$0.23\lambda_g \times 0.62\lambda_g$	3/1	No
19 Filter B	1.65/5.25	35.1/7.2	20/25	0.41/1.1	$0.33\lambda_g \times 0.03\lambda_g$	2/2	No
21	2.4/3.5	6.7/7.2	15/14	2/1.9	$0.16\lambda_g \times 0.25\lambda_g$	6/2/2/2	No
	5.2/5.8	6.9/5.3	21/16	1.9/1.96			
This work (A)	1.875/5.52	43.2/10.5	12/25	0.39/0.87	$0.05\lambda_g \times 0.56\lambda_g$	1/3	Yes
This work (B)	1.63/4.46	31.9/33.0	15/12	0.70/0.12	$0.09\lambda_g \times 0.56\lambda_g$	1/2	Yes

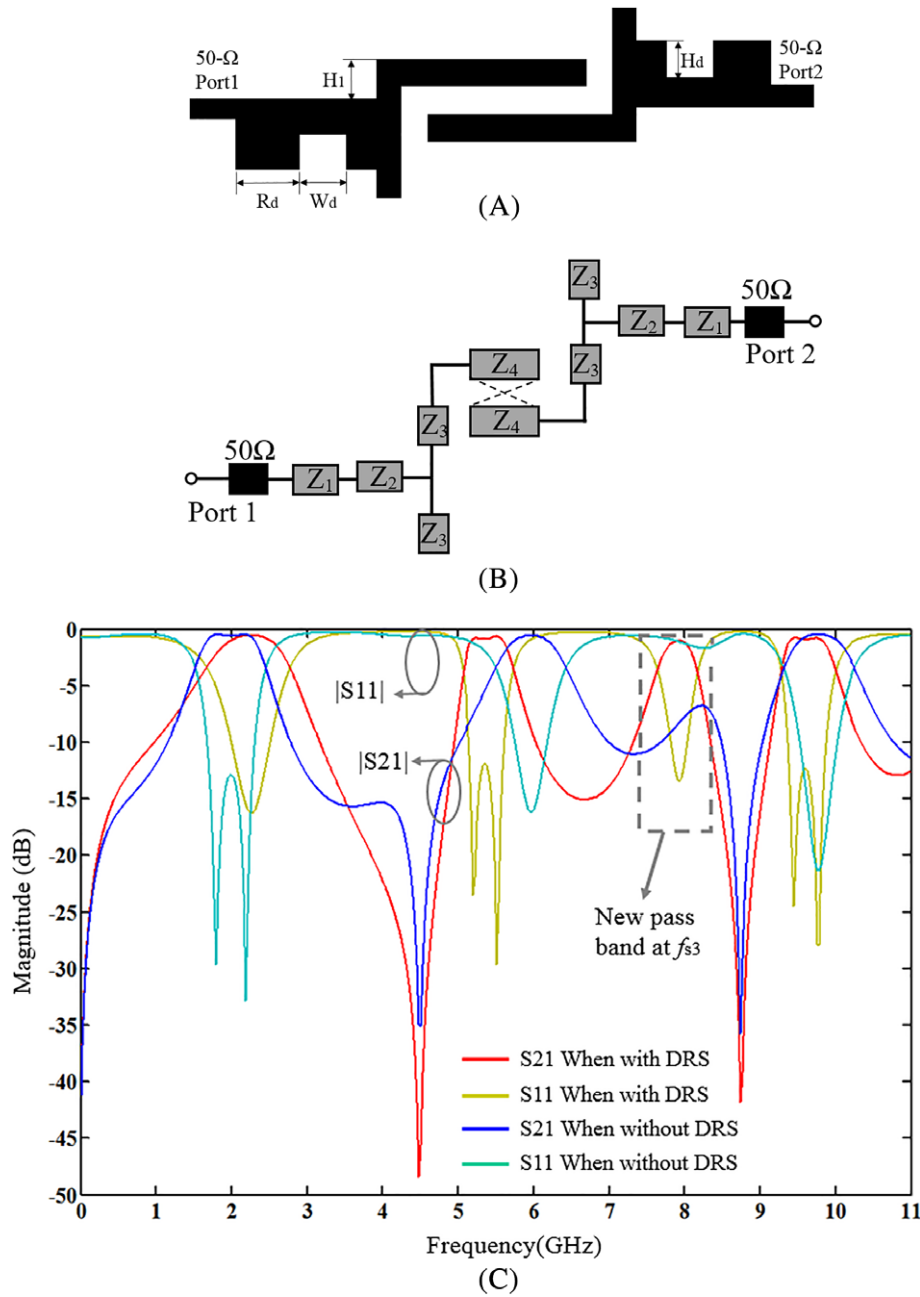


FIGURE 20 Schematic diagram of the modified SS-ASIR filter with DRS: (A) structure. (B) Equivalent circuit and coupling routing scheme for the SS-ASIR filter with DRS. (C) The frequency response comparison of SS-ASIR filter with DRS and without DRS

Mobile Communication (GSM: 1800 MHz), and Universal Mobile Telecommunication System (UMTS: 1710-1880 MHz etc.). The second pass band ranges from 3.66 to 5.46 GHz with central frequency of 4.46 GHz, bandwidth of 1.8 GHz and fractional band width (FBW) of 33.0%. It can be applied in IEEE802.11a WLAN applications including 5G Wi-Fi. Moreover, good isolation is achieved between the two pass bands to eliminate signal interference between dual-bands. The stop band ranges from 2.12 to 3.5 GHz with -10 dB suppression. Due to the adoption of parallel uncoupled microstrip lines, an extra transmission zero near f_{s3} and f_{s4} is realized. A wide upper stop band ranging from

5.83 to 9.35 GHz with -10 dB suppression level is generated, which can be seen in Figure 19.

The parameters of the modified SS-ASIR with parallel uncoupled microstrip lines are shown in Table 2. A comparison of the performance of the modified SS-ASIR filter with ICCLs and PUMs with previous work is shown in Table 3.

3.4 | The modified SS-ASIR filter with defected rectangular structure (DRS)

The topological structure of the proposed modified skew-symmetrical asymmetric SIR Filter with defected structure is

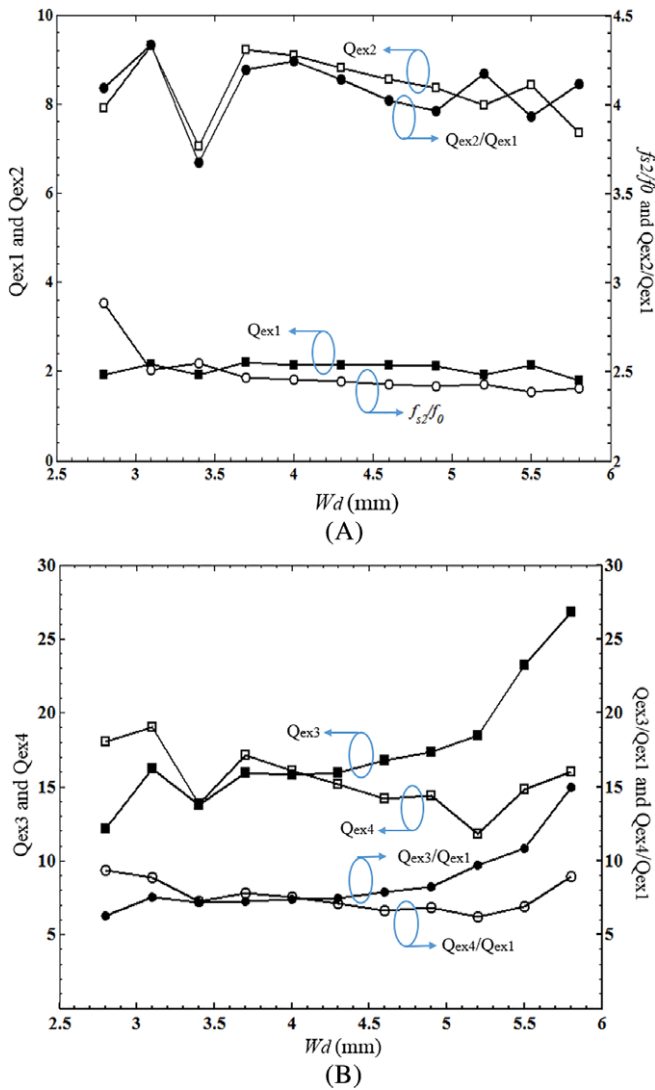


FIGURE 21 W_d 's effect on SS-ASIR filter with DRS. (A) Q_{ex1} , Q_{ex2} , f_{s2}/f_0 and Q_{ex2}/Q_{ex1} vs against W_d . (B) Q_{ex3} , Q_{ex4} , Q_{ex3}/Q_{ex1} and Q_{ex4}/Q_{ex1} vs against W_d

shown in Figure 20. In contrast to the original skew-symmetrical asymmetric SIR filter, this filter has a defected rectangular structure (DRS) in each low impedance line, of width and length W_d and H_d , respectively. Its relative distance to the end of the feed line is R_d . By utilizing the defected rectangular structure, the performance-degraded frequency response at f_{s3} can enhance the frequency response and a new wide pass band can be excited centered at f_{s3} . The frequency response comparison between the modified SS-ASIR filter with and without DRS is plotted in Figure 20C. By this means, a quad-band filter can be formed by adopting the defected rectangular structure in the SS-ASIR filter.

Again, the same procedure applied to achieve the equivalent circuit elements used in Figures 10C and 14B, is adopted for the SS-ASIR filter with DRS and without DRS as shown in Figure 20B. The impedance values of the

transmission lines are: $Z_1 = 34.6069 \Omega$, $Z_2 = 49.6435 \Omega$, $Z_3 = 23.5845 \Omega$, and $Z_4 = 67.0065 \Omega$.

Figure 21 plots the W_d 's effect on SS-ASIR filter with DRS. In (a), when W_d varies from 2.5 to 6 mm, f_{s2}/f_0 decreases while Q_{ex1} remains almost the same: Q_{ex2} and Q_{ex2}/Q_{ex1} fluctuate in this process. This means f_{s2} does not follow the rules of invariance of resonant frequency location in the SS-ASIR coupled structure any more. In (b), Q_{ex3} varies from 12.1 to 26.8 and Q_{ex4} varies from 18.1 to 16 when W_d ranges from 2.5 to 6 mm, with Q_{ex3}/Q_{ex1} increasing continuously.

From EM simulations, it is noted that not all f_{s2} , f_{s3} , and f_{s4} in SS-ASIR coupled structures with DRS obey the rules of invariance of resonant frequency location: frequency shifting exists among all four pass bands compared to the situation that there is no DRS. This is because the basic structure of SS-ASIR coupled pairs is modified by the defected rectangular structure.

The simulated S-parameters, measured S-parameters and photograph of the hardware realization of the designed quad-wideband SS-ASIR filter with DMS are plotted in Figure 22. There is good agreement between the simulated and measured results and the discrepancies are attributed to loss, fabrication errors and so on. It can be seen that dual wide bands are realized with good in-band return loss performance. The first pass band ranges from 1.64 to 2.62 GHz with central frequency of 2.13 GHz, bandwidth of 980 MHz and fractional band width (FBW) of 46.0%. It can be applied in the Global System for Mobile Communication (GSM: 1800 MHz/1900 MHz), Universal Mobile Telecommunication System (UMTS: 1710-1880/1850-1990/1920-2170 MHz etc.), ISM (Industrial, Scientific and Medical band: 2.4 GHz), and WLAN IEEE 802.11b/g/n applications including 2.4 GHz Wi-Fi. The second pass band ranges from 4.95 to 5.55 GHz with central frequency of 5.25 GHz, bandwidth of 600 MHz and fractional band width (FBW) of 11.4%. It can be used in IEEE802.11a WLAN applications. The third pass band ranges from 7.51 to 7.86 GHz with central frequency of 7.685 GHz, bandwidth of 350 MHz FBW of 4.6%, and can be used in electronic countermeasure (ECM) applications. The fourth pass band ranges from 9.06 to 9.56 GHz with central frequency of 9.31 GHz, bandwidth of 500 MHz and FBW of 5.4%, suitable for X-band applications.

Moreover, good isolation is achieved between four pass bands, eliminating signal interference. The -10 dB suppression level stop bands range from 3.05 to 4.78 GHz between the first and second pass band, 5.77 to 7.20 GHz between the second and third pass band, and 8.04 to 8.889 GHz between the third and fourth pass band. Moreover, two transmission zeroes located at 4.26 GHz and 8.46 GHz are formed to further enhance frequency selectivity, as shown in

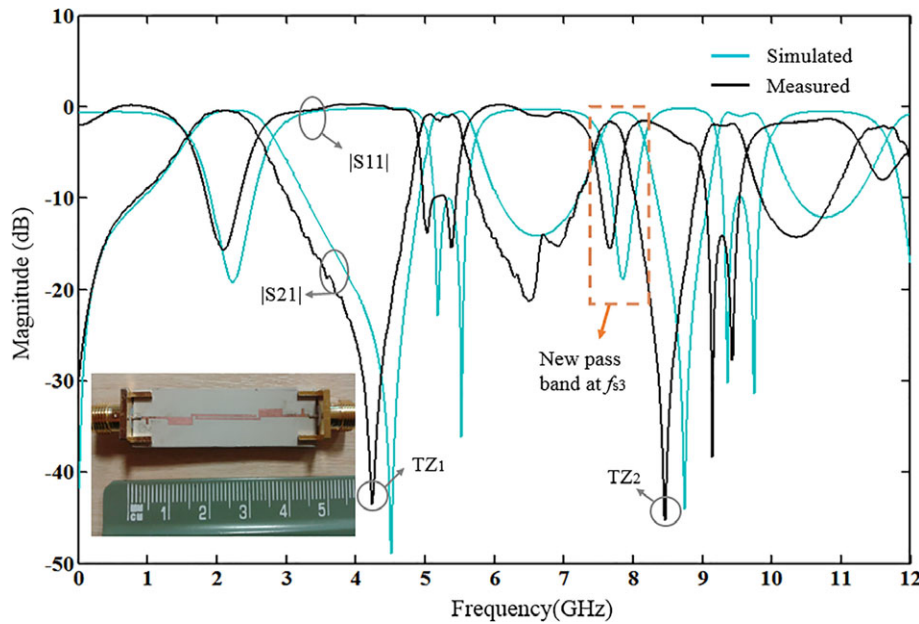


FIGURE 22 Simulated, measured results and photograph of the hardware realization of the modified SS-ASIRs with DMS

Figure 22. The parameters of modified SS-ASIR with DMS are shown in Table 2. The size of the modified SS-ASIRs with DMS is $0.09\lambda_g \times 0.56\lambda_g$, where λ_g is the guide wavelength.

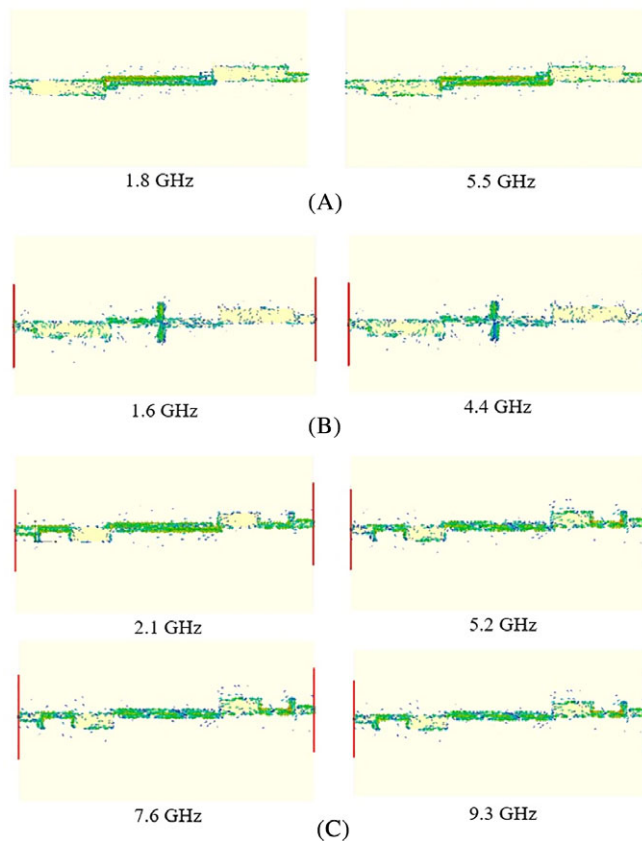


FIGURE 23 Current distribution for the designed filters. (A) SS-ASIRs with ICCLs. (B) SS-ASIRs with PUMs. (C) SS-ASIRs with DMS

3.5 | Surface current distribution for the proposed filters

For further validation by using the CST software simulator, Figure 23 elaborates the current distribution of the reported pass band filters at the resonant frequencies.

As shown in Figure 23A, the electric field is mainly distributed near the interdigital cross-coupled lines, with maximum current density 60 and 58 A/m at 1.8 and 5.5 GHz, respectively. But for Figure 23B, the electric field is mainly distributed near the parallel uncoupled microstrip lines, with maximum current densities 58 and 57 A/m at 1.6 and 4.4 GHz, respectively. On the other hand, as seen from Figure 23C, most of the currents are around the defected rectangular structures and the two coupled transmission lines with maximum current densities 60 A/m at 2.1, 5.2, 7.6, and 9.3 GHz. It is significant that the proposed designs can be easily developed to handle and permit reconfigurability^{24,25} and can be easily integrated with antenna designs,²⁶ to create the so-called “filtenna”.²⁷

4 | CONCLUSION

Multi-standard dual-wideband and quad-wideband filters based on the detailed analysis of the simple asymmetric stepped-impedance resonator unit and of the skew-symmetrical asymmetric stepped-impedance resonator coupled pair have been presented. By utilizing a novel modified skew-symmetrical asymmetric stepped-impedance resonator coupled pair with interdigital cross-coupled lines and parallel uncoupled microstrip lines, the dual-band filters for the first time among recently proposed dual-wideband filters

realize dual-wideband with wide stop band restrictions. Their bandwidths are controllable by tuning relative parameters. By introducing a defected microstrip structure, a frequency band nearby the third spurious frequency is formed, resulting in a quad-wideband filter. The proposed dual-wideband and quad-wideband modified skew-symmetrical asymmetric stepped-impedance resonator filters cover communication applications including Global Positioning System, Global System For Mobile Communication, The Universal Mobile Telecommunications System, industrial, scientific and medical band, and IEEE 802.11 a/b/g/n/ac. The filters' measured results agree well with simulated results and theoretical predictions. The good in-band and out-of-band performance, compact size and simple structure make the proposed filters very promising for applications in future multi-standard wireless communication.

ACKNOWLEDGMENTS

This project has received funding from the European Union's Horizon 2020 research and innovation programme under grant agreement H2020-MSCA-ITN-2016 SECRET-722424.

ORCID

Yasir I. A. Al-Yasir  <https://orcid.org/0000-0002-7859-3550>

REFERENCES

- Liu HW, Ren BP, Li S, et al. High-temperature superconducting bandpass filter using asymmetric stepped-impedance resonators with wide-stopband performance. *IEEE Trans Appl Superconduct*. 2015;25(5):1-6.
- Tu YX, Guo XR, Wang CH, Jin J. An improved 860–960MHz fully integrated CMOS power amplifier designation for UHF RFID transmitter. *Int J Electron Commun*. 2013;67(7):574-577.
- Chang YC, Kao CH, Weng MH, Yang RY. Design of the compact dual-band bandpass filter with high isolation for GPS/WLAN applications. *IEEE Microw Wireless Compon Lett*. 2009;19(12):780-782.
- Kim CH, Chang K. Independently controllable dual-band bandpass filters using asymmetric stepped-impedance resonators. *IEEE Trans Microw Theory Techn*. 2011;59(12):3037-3047.
- Wu HW, Yang RY. A new quad-band bandpass filter using asymmetric stepped impedance resonators. *IEEE Microw Wireless Compon Lett*. 2011;21(4):203-205.
- Kim CH, Chang K. Wide-stopband bandpass filters using asymmetric stepped-impedance resonators. *IEEE Microw Wireless Compon Lett*. 2013;23(2):69-71.
- Chang YC, Kao CH, Weng MH, Yang RY. Design of the compact wideband bandpass filter with low loss, high selectivity and wide stopband. *IEEE Microw Wireless Compon Lett*. 2008;18(12):770-772.
- Al-Yasir Y, Tu Y, Ojaroudi Parchin N, et al. Mixed-coupling multi-function quint-wideband asymmetric stepped impedance resonator filter. *Microw Opt Tech Lett*. 2019;0(0):1-4.
- Zhang RQ, Zhu L, Luo S. Dual-mode dual-band bandpass filter using a single slotted circular patch resonator. *IEEE Microw Wireless Compon Lett*. 2012;22(5):233-235.
- Zhang RQ, Zhu L. Synthesis and design of wideband dual-band bandpass filters with controllable in-band ripple factor and dual-band isolation. *IEEE Trans Microw Theory Techn*. 2013;61(5):1820-1828.
- Xu J, Wu W, Miao C. Compact microstrip dual-/tri-/quad-band bandpass filter using open stubs loaded shorted stepped-impedance resonator. *IEEE Trans Microw Theory Techn*. 2013;61(9):3187-3199.
- Zhang RQ, Zhu L. Synthesis of dual-wideband bandpass filters with source-load coupling network. *IEEE Trans Microw Theory Techn*. 2014;62(3):441-449.
- Li J, Huang SS, Zhao JZ. Compact dual-wideband bandpass filter using a novel Penta-mode resonator (PMR). *IEEE Trans Microw Theory Techn*. 2014;24(10):668-670.
- Sanchez-Soriano MA, Gomez-Garcia R. Sharp-rejection wide-band dual-band bandpass planar filters with broadly-separated passbands. *IEEE Microw Wireless Compon Lett*. 2015;25(2):97-99.
- Liu HW, Wen P, Wang XM, et al. Dual-band high-temperature superconducting hairpin-resonator bandpass filter based on two pairs of nondegenerate modes. *IEEE Trans Appl Supercond*. 2015;25(3):1-4.
- Serrano ALC, Corraera FS, Vuong T-P, Ferrari P. Synthesis methodology applied to a tunable patch filter with independent frequency and bandwidth control. *IEEE Trans Microw Theory Techn*. 2012;60(3):484-493.
- Hong JS, Lancaster MJ. *Microstrip Filter for RF/Microwave Applications*. New York: Wiley; 2001.
- Tu Y, Ali A, Elmegri F, et al. Novel multi-standard dual-wide band polygon SLSIR filter. *2015 Internet Technologies and Applications (ITA)*, pp. 434-438, 2015.
- Xu J, Wen W, Miao C. Compact and sharp skirts microstrip dual-mode dual-band bandpass filter using a single quadruple-mode resonator (QMR). *IEEE Trans Microw Theory Techn*. 2013;61(3):1104-1113.
- Matthaei GL, Young L, Jones EMT. *Microstrip Filters, Impedance-Matching Network, and Coupling Structures*. Norwood, MA: Artech House; 1980.
- Yan T, Tang X-H, Wang J. A novel quad-band bandpass filter using short stub loaded E-shaped resonators. *IEEE Microw Wireless Compon Lett*. 2015;25(8):508-510.
- Al-Yasir YIA, Abd-Alhameed RA, Noras J, Abdulkhaleq A, Ojaroudi Parchin N. Design of very compact combline band-pass filter for 5G applications. *Loughborough Antennas & Propagation Conference*, 2018, Loughborough, UK.
- CST Microwave Studio, <http://www.cst.com>.
- Yuceer M. A reconfigurable microwave combline filter. *IEEE Trans Circuits Syst II Express Briefs*. 2016;63(1):84-88.
- Al-Yasir Y, Ojaroudi Parchin N, Abd-Alhameed R, Abdulkhaleq A, Noras J. Recent progress in the design of 4G/5G reconfigurable filters. *Electronics*. 2019;8(1).
- Al-Yasir YIA, Abdullah A, Mohammed H, Abd-Alhameed R, Noras J. Design of frequency-reconfigurable multiband compact

antenna using two PIN diodes for WLAN/WiMAX applications. *IET Microw Antennas Propag.* 2017;11(8):1098-1105.

27. Atallah H, Abdul Rahman A, Yoshitomi K, Pokhare P. Compact frequency reconfigurable filtennas using varactor loaded t-shaped and h-shaped resonators for cognitive radio applications. *IET Microw Antennas Propag.* 2016;10(9):991-1001.

AUTHOR BIOGRAPHIES



Yasir I. A. Al-Yasir received the BSc and MSc degrees in Electrical Engineering from University of Basra, Basra, Iraq in 2012 and 2015, respectively. Since January 2018, he has appointed as an Early-Stage Researcher (ESR) at School of Electrical Engineering

and Computer Science, Bradford University, UK. Currently, he is working as ESR 6 of 13 ESRs of 8 research groups, spread across 4 leading Universities/research institutions and 4 industrial partners in 5 different European countries, targeting a Secure Network Coding for Reduced Energy Next Generation Mobile Small Cells (SECRET) the Horizon 2020 Marie Skłodowska-Curie Actions. In addition, he is currently working toward his PhD degree within the Radio Frequency and sensor design research group at Bradford University. His main interests are RF antennas, filters and microwave circuit designs. He has published many book chapters and papers on aspects of wireless communications.



Yuxiang Tu has received the PhD degree in Electrical Engineering from the School of Engineering and Informatics, University of Bradford in 2016. He is with the Radio Frequency, Communication and Network research group, School of Electrical Engineering

and Computer Science, Bradford University, Bradford, UK. He has authored and co-authored many technical journal and conference papers. His research interests include multiband/UWB microwave filters and antennas.



Naser Ojaroudi Parchin was born in Germi, Iran, in 1986. He is currently pursuing the PhD degree with the University of Bradford, UK, where he is also a Research Assistant. He has authored or co-authored many technical journal and conference papers with

23h-index and 55 i10-index. His research interests include multiband/UWB antennas, mm-wave phased

array antennas, MIMO/diversity antennas, Fabry resonators, microwave filters, reconfigurable structures, and electromagnetic wave propagation. He is also a Reviewer in many journals, such as the IEEE ACCESS, the IEEE AWPL, and the IET MAP.



Ahmed M. Abdulkhaleq was born in Mosul, Iraq. He received his BSc degree in Communications Engineering (Class Ranking: first) from the University of Mosul, Iraq in 2009. In 2010 to 2011, he worked as an engineer at college of Electronics, University of Mosul, Iraq. In 2013, he was awarded MSc degree in Personal Mobile and Satellite Communications (with distinction) from the University of Bradford. Since then, he worked as a lecturer at the University of Nineveh. He is currently working toward his PhD degree within SARAS Technology and the RF and Microwave design research group at Bradford University. He contributed to many international journal and conference papers. His research interests include energy efficient RF power amplifiers, digital signal processing (DSP), antenna array processing, and reconfigurable transceivers.



Jamal Kosha was born in Tripoli, Libya. He received his BSc degree in Electronics and Computer Engineering from Al Fatah University, Tripoli, Libya in 1994. He had worked as lecturer assistant for 1 year in the same university. He had worked as the Head

of the Statistics & Information Office in Almadar Telecom Company for 2 years. He was appointed as the Head of Corporate Development Office in Almadar Aljadid Telecom Company from 2012 to 2015. He later received his MSc degree in Human Resources Management in 2017 from University of Salford. Since July 2017, he joined the Faculty of Engineering and Informatics at University of Bradford to pursue his PhD research degree in the field of Wireless and Mobile Communications Systems and its Implementation on FPGA.



Atta Ullah was born in Mardan (KPK) Pakistan in 1979. He received his BSc and MSc degrees in Electronics Engineering from University of Peshawar, Pakistan in 1999 and 2002, respectively and after this he received MSc in communication engineering from University of York, UK in 2008. He has worked as Electronics Design Engineer in Creative Electronics in Pakistan and

worked as Lecturer at University of Hail, Saudi Arabia. Now he is currently working toward his PhD degree within the radio frequency and sensor design research group. His research interests include simulation, design, and implementation of front-end antenna systems for millimeter wave communications.



Raed A. Abd-Alhameed (M'02-SM'13) received the BSc and MSc degrees in Electrical Engineering from Basrah University, Basrah, Iraq, in 1982 and 1985, respectively, and the PhD degree in Electrical Engineering from the University of Bradford, UK, in 1997. He has also been a Research Visitor with Glyndwr University, Wrexham, UK, since 2009. He is currently a Professor of electromagnetic and radio frequency engineering with the University of Bradford. He is the Leader of radio frequency, propagation, sensor design, and signal processing. He leads the Communications Research Group, School of Engineering and Informatics, Bradford University, for years. He is investigator of several funded applications. He has published more than 500 academic journal and conference papers, and books. His research interests include computational methods and optimizations, wireless and mobile communications, sensor design, signal processing, EMC, propagations, antennas, beam steering, energy-efficient PAs, and RF predistorter design applications.



James M. Noras is currently a Senior Lecturer with the School of Engineering, Design and Technology, University of Bradford, UK. He is also the Director of five internationally franchised BEng and MSc courses in electrical and electronic engineering, has successfully supervised 18 PhD students, and is currently supervising the research of 3 PhD students. He has published 50 journal papers and 85 conference papers, in fundamental semiconductor physics, analog and digital circuit design, digital signal processing, and RF system design and evaluation. His main research interests include digital system design and implementation, DSP and coding for communication systems, and localization algorithms for mobile systems. He is a member of the Institute of Physics and a Chartered Physicist.

How to cite this article: Al-Yasir YIA, Tu Y, Ojaroudi Parchin N, et al. New multi-standard dual-wideband and quad-wideband asymmetric step impedance resonator filters with wide stop band restriction. *Int J RF Microw Comput Aided Eng*. 2019;e21802. <https://doi.org/10.1002/mmce.21802>